Waste Disposal & Sustainable Energy (2022) 4:105–116
https://doi.org/10.1007/s42768-022-00096-1

ARTICLE

Solvothermal preparation of Mn-based catalysts for simultaneous removal of 1,2-dichlorobenzene and furan

Juan Qiu[1] · Yaqi Peng[1] · Minghui Tang[1] · Shengyong Lu[1] · Xiaodong Li[1] · Jianhua Yan[1]

Received: 16 February 2022 / Revised: 24 March 2022 / Accepted: 8 April 2022 / Published online: 27 June 2022

Abstract

In this study, Mn-based bimetallic oxide catalysts were synthesized via the solvothermal method. Different metals (Ce, Co and Fe) exhibited a great impact on the physicochemical properties of catalysts, resulting in different catalytic activities for the simultaneous removal of 1,2-dichlorobenzene (1,2-DCB) and furan, as a model of polychlorinated dibenzodioxins and dibenzo-furans (PCDD/Fs). Fe–MnOx presented the best catalytic activity, with a removal efficiency of 62% for 1,2-DCB and 100% for furan at 240 °C. Several analytical techniques were employed, namely, Brunauer–Emmett–Teller (BET), X-ray diffraction (XRD), scanning electron microscope (SEM), X-ray photoelectron spectroscopy (XPS), H_2 temperature-programmed reduction (H_2-TPR), and ammonia temperature programmed desorption (NH_3-TPD). Compared with pure MnOx catalysts, Fe–MnOx shows a higher specific surface area of 117.9 m^2/g. SEM observations showed flower-like nanosheet structures for Fe–MnOx. XPS analysis indicated that Mn^{4+}/Mn^{3+} and active oxygen play the key roles in the catalytic oxidation of 1,2-DCB and furan. The catalytic activity, selectivity and stability of Mn-based bimetallic oxide catalysts for the oxidation of 1,2-DCB and furan were tested. Competition exists between 1,2-DCB and furan such that the adsorption of furan occurs prior to 1,2-DCB.

Keywords Polychlorinated dibenzodioxins and dibenzo-furans · 1,2-dichlorobenzene · Catalytic oxidation · Fe–MnOx · Product analysis

Introduction

The incineration and combustion processes of waste such as municipal and medical waste emit polychlorinated dibenzodioxins and dibenzo-furans (PCDD/Fs), which have very stable structures consisting of three aromatic rings [1]. 1,2-dichlorobenzene (1,2-DCB) has been chosen as a model compound of PCDD/PCDFs (polychlorinated dibenzofuran), while furan has already been studied as a model of the central ring of a PCDFs. 1,2-DCB and furan are chosen as model compounds of PCDD/PCDFs to evaluate the activity of the catalysts in the oxidation of the chlorinated aromatic ring and oxygenated aromatic ring [2, 3]. Catalysis is the most promising solution, because it can directly degrade these pollutants to form harmless products. Numerous types of noble metal and transition metal oxide catalysts have been referenced in the literature. However, the disadvantages of noble metals, compared with transition metal oxides, include higher costs, and deactivation due to their sensitivity to poisoning and sintering at higher temperatures. Transition metal oxide catalysts have several advantages, including higher thermal stability, lower costs, and the possibility of fabrication in high-surface area porous powders [4].

Transition metal oxide-based catalysts typically use one or more transition metal oxides as active phases, such as supported VOx-based catalysts, MnOx-based catalysts, and FeOx-based catalysts [5]. Nevertheless, the drawbacks of industrial VOx-based catalysts, such as high working temperatures (300–400 °C) and the toxicity of VOx constrain their practical application at low temperatures. Among the transition metal oxides, Mn–Ce oxides present high activity in catalytic combustion of chlorobenzene [5–7]. Mn and Ce oxides possess variable oxidation states that contribute to an excellent oxygen storage capacity and oxygen mobility

✉ Minghui Tang
lytmh1214@zju.edu.cn

✉ Shengyong Lu
lushy@zju.edu.cn

[1] State Key Laboratory for Clean Energy Utilization, Institute for Thermal Power Engineering, Zhejiang University, Hangzhou 310027, China

[8]. Meanwhile, iron oxide has abundant active sites that are adsorbed sites of chlorinated organics [5]. In recent studies, Ma et al. reported that Fe–Mn mixed oxides prepared by facile template fabrication were used for catalytic oxidation of 1,2-DCB and exhibited high catalytic activity [9]. Cai et al. reported that Mn-modified Co_3O_4 catalysts with spinel structures prepared by precipitation were used in the catalytic combustion of 1,2-DCB, which presented the highest activity and stability [10].

Wang et al. reported that the morphology of Ce–Mn oxide catalysts had a great effect on the activity and stability, and that nano-rods showed better activity than nano-sheets or nano-particles for chlorobenzene (CB) oxidation [11, 12]. Tang et al. found that the addition of Ce and Fe to manganese oxide catalysts enhanced the specific surface area and promoted the catalytic oxidation activity of 1,2-DCB[7]. Khaleel et al. reported that the activity of the Fe–Ti mixed oxide catalyst prepared via the sol–gel method exhibited unique activity for the complete oxidation of chlorobenzene at relatively low temperatures [13]. Qi et al. reported that Mn–Fe/TiO_2 catalysts yielded nearly 100% NO conversion at 120 °C, indicating that iron doping enhanced the catalyst surface area [14]. Zhang et al. noted that Ce–MnOx synthesized by the hydrothermal method presented better catalytic oxidation activity of toluene than catalysts prepared by impregnation and co-precipitation [15]. Shi et al. reported that Mn-based bimetallic oxide catalysts prepared by the solvothermal method presented significant variation and Co–MnOx exhibited the best deNOx activity and SO_2 tolerance [6].

In this work, common metals, namely, Ce, Co, and Fe were selected and Mn-based bimetallic oxide catalysts were synthesized via a solvothermal method. The physical and chemical properties of the catalysts resulting from doping by different metals were investigated. The catalytic activity, selectivity and stability of Mn-based bimetallic mixed oxides for the oxidation of 1,2-DCB and furan were evaluated, then the catalysts were characterized by different methods. Fe–MnOx and Ce–MnOx were adopted for the simultaneous removal of 1,2-DCB and furan.

Materials and methods

Materials

The glycerol ($C_3H_5(OH)_3$), isopropanol ($(CH_3)_2CHOH$), manganese acetate ($Mn(CH_3COOH)_2{\cdot}4H_2O$), cerous nitrate ($Ce(NO_3)_3{\cdot}6H_2O$), cobalt nitrate ($Co(NO_3)_2{\cdot}6H_2O$), and ferric nitrate ($Fe(NO_3)_2{\cdot}9H_2O$) were purchased from Sinopharm Group (Beijing, China). All chemical reagents were of analytical grade.

Catalyst preparation

MnOx and Mn-based bimetallic oxide catalysts with different metal dopants (Ce, Co, Fe) were prepared via a simple solvothermal approach. Taking Ce–MnOx as an example, 2 mmol of $Mn(CH_3COOH)_2$ and 1 mmol $Ce(NO_3)_3$ were dissolved in a mixed homogeneous solution of glycerol ($C_3H_5(OH)_3$) (10 mL) and isopropanol ($(CH_3)_2CHOH$) (70 mL) under constant stirring. Subsequently, the above mixed solution was transferred into a 100-mL stainless-steel autoclave. The reaction kettle was heated in an oven held at 180 °C for 18 h and then cooled to room temperature. The precipitate was filtered, washed with ethanol and deionized water, dried at 80 °C overnight and finally calcined at 450 °C for 4 h in air with a heating rate of 2 °C/min. All the above catalysts were pellet-pressed and sieved to 40–60 mesh before further tests were carried out. Four catalysts, including three doped with different metals, were prepared by this procedure, and noted as MnOx, Ce–MnOx, Co–MnOx, and Fe–MnOx.

Characterization

The surface area and pore structures of the samples were measured by N_2 isotherm curves performed on a Micromeritics TriStar 3020 and calculated with the Brunauer–Emmett–Teller (BET) and Barrett–Joyner–Hallend (BJH) methods. The morphologies of the catalysts were analyzed by a SU-8010 scanning electron microscope (SEM, Hitachi, Japan) and transmission electron microscope (TEM, HT-7700, Hitachi, Japan). X-ray diffraction (XRD) was performed by a Philips Model XD-98 X-ray diffractometer (XRD) with Cu Kα radiation (λ=0.15406 nm) and a scanning rate of 0.02°/min (X'Pert PRO, PANalytical, Almelo, Netherlands). X-ray photoelectron spectroscopy (XPS) spectra were recorded onan ESCAlab 250Xi with Al Kα X-rays. The binding energies were calibrated by the C 1s peak at 284.5 eV. A chemisorption apparatus with a TCD detector (Micromeritics Autochem II 2920, Micromeritics, Norcross, GA, USA) was used for H_2 temperature-programmed reduction (H_2-TPR) and ammonia temperature programmed desorption (NH_3-TPD) experiments.

Catalytic activity test

The catalyst activity test was performed in a quartz tube reactor with an inner diameter of 0.80 cm and using the 0.2 g sample of 40–60 mesh. The temperature of the reactor was controlled with an electric furnace and was raised stepwise from 120 °C to 360 °C. 1,2-DCB was generated by the bubbling method and the initial concentration of the

1,2-DCB was 50 ppm. The initial concentration of the furan was 100 ppm. The volume flow was controlled at 100 mL/min by mass controllers with 10 vol% O_2 and N_2 as the balance gas. The outlet gas was analyzed using a gas chromatograph (GC 9790, FULI, Wenling, China) equipped with a 30-m column (DB-5) and a flame ionization detector (FID). The removal efficiency (RE) for 1,2-DCB and furan were calculated by using Eqs. (1) and (2)

$$\mathrm{RE}\ (\%) = \frac{[1,2\text{ - DCB}]_{\mathrm{inlet}} - [1,2\text{ - DCB}]_{\mathrm{outlet}}}{[1,2\text{ - DCB}]_{\mathrm{inlet}}} \times 100\%, \quad (1)$$

$$\mathrm{RE}\ (\%) = \frac{[\mathrm{Furan}]_{\mathrm{inlet}} - [\mathrm{Furan}]_{\mathrm{outlet}}}{[\mathrm{Furan}]_{\mathrm{inlet}}} \times 100\%, \quad (2)$$

The yields of CO and CO_2 were calculated using Eqs. (3)–(5), respectively, as follows:

$$Y_{\mathrm{CO}}\ (\%) = \frac{[\mathrm{CO}]_{\mathrm{outlet}}}{6[1,2\text{ - DCB}]_{\mathrm{inlet}}} \times 100\%, \quad (3)$$

$$Y_{\mathrm{CO_2}}\ (\%) = \frac{[\mathrm{CO_2}]_{\mathrm{outlet}}}{6[1,2\text{ - DCB}]_{\mathrm{inlet}}} \times 100\%, \quad (4)$$

$$Y_{\mathrm{CO+CO_2}}(\%) = \frac{[\mathrm{CO} + \mathrm{CO_2}]_{\mathrm{outlet}}}{6[1,2\text{ - DCB}]_{\mathrm{inlet}}} \times 100\%. \quad (5)$$

The concentrations of CO_2/CO and HCl in the effluent gas were analyzed using a DX4000 Gasmet FT-IR gas analyzer (DX4000, Dekati Ltd., Beijing, China). A gas chromatography and mass spectrometry (GC/MS) analyzer (an Agilent 7890A gas chromatograph and an Agilent 5975C mass spectrometer, Agilent, Beijing, China) identified the intermediate products. The off-gases were first captured with a Tenax-GR for 30 min and then released into a thermal desorption instrument (PERSEE-TP7, Agilent, Beijing, China) connected to a GC/MS analyzer.

Results and discussion

BET

The corresponding S_{BET}, V_{p}, and D_{p} are listed in Table 1. It can be seen that the BET specific surface area of Fe–MnOx (117.9 m^2/g) was much higher than those of MnOx (54.6 m^2/g), Ce–MnOx (67.5 m^2/g) and Co–MnOx (46.6 m^2/g). The higher specific surface area was considered to be a key contributing factor to the high catalytic activity [15]. As shown in Fig. 1, the porosities of the catalysts were measured by the N_2 adsorption technique. The isotherms of

Table 1 Summary of textural parameters of the samples

Sample	S_{BET} (m^2/g)	V_{p} (cm^3/g)	D_{p} (nm)
MnOx	54.6	0.6462	23.65
Ce–MnOx	67.5	0.1192	3.533
Co–MnOx	46.6	0.246	10.57
Fe–MnOx	117.9	0.3021	5.125

BET Brunauer–Emmett–Teller

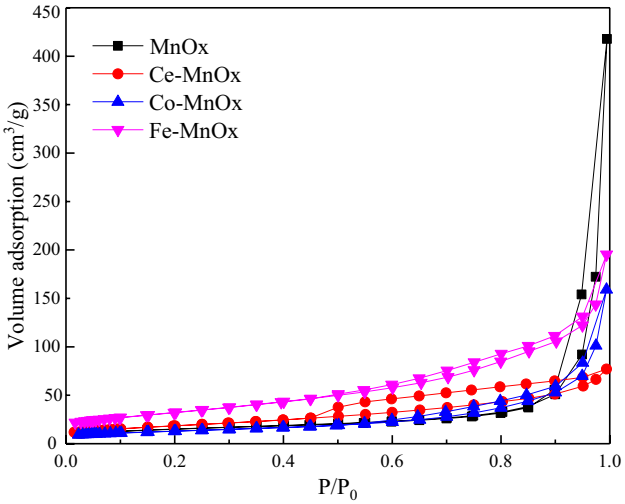

Fig. 1 N_2 adsorption–desorption isotherms of the catalysts

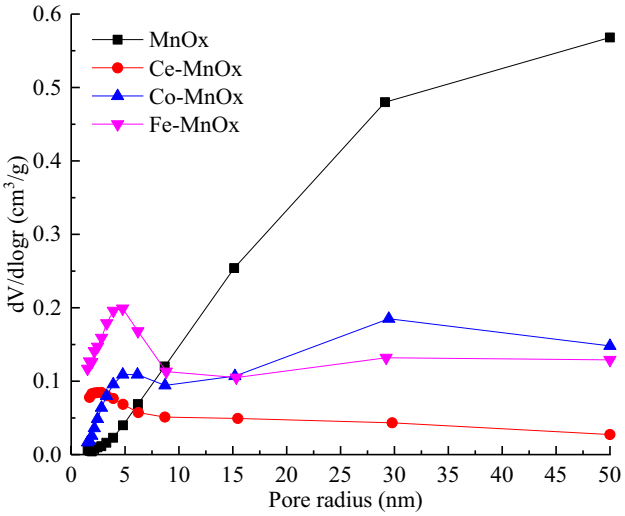

Fig. 2 BJH pore-size distribution of the catalysts. *BJH* Barrett–Joyner–Hallend

MnOx and Co–MnOx catalysts belong to type III according to the IUPAC recommendation [16]. An increase in relative pressure > 0.9 could be observed, indicating the presence of large mesopores [7]. The isotherms of Ce–MnOx and Fe–MnOx resemble type IV with a well-defined type

H3 hysteresis loop, suggesting the presence of a narrow distribution of mesoporous diameters [17]. Figure 2 presents the BJH pore-size distribution of the catalysts. It was observed that the pore size of MnOx was larger than the other catalysts. The pore sizes of Ce–MnOx, Co–MnOx, and Fe–MnOx were mainly distributed in the range of 2–10 nm and showed different pore-size distribution peaks. It was noted that Fe–MnOx exhibited more mesoporous structures than those of other catalysts, which might be a reason for the higher activity.

XRD

The crystal phases of the all catalysts in the range of 10°–80° were determined by XRD characterization and the results are shown in Fig. 3. For the pure MnOx catalyst, 12 peaks appeared at 2θ = 18.1°, 21.6°, 28.7°, 31.9°, 32.5°, 36.3°, 38.3°, 47.8°, 49.1°, 55.1°, 60.5°, and 66.1°, respectively. The peaks at 18.1°, 31.9°, 36.3°, and 38.3° were assigned to the main phase of crystallinity Mn_3O_4, and the peaks near 2θ = 21.6°, 28.7°, 47.8°, 60.5° were the typical diffractions of the pyrolusite MnO_2. The peaks at 32.5°, 49.1°, 55.1°, and 66.1° were assigned to the diffraction peaks of the hausmannite Mn_2O_3. For the Ce–MnOx catalyst, the reflections at 28.6° and 47.4° belong to MnO_2 and CeO_2, respectively [18]. For the Co–MnOx catalyst, characteristic diffraction peaks at 18.1° and 36.3° as well as 44.5° corresponded to MnO_2 and Co_3O_4, respectively [10]. For the Fe–MnOx sample, the reflections at 35.6° and 43.2° were assigned to the main phase of Fe_3O_4, and the reflections at 63.2° was ascribed to Fe_2O_3 [9]. Previous studies reported that the existence of the crystal structures of FeOx and Fe–MnOx solid solutions could increase the catalytic oxidation performance [8, 12].

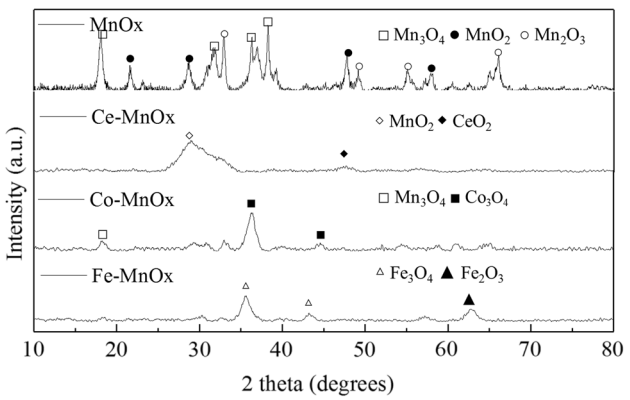

Fig. 3 XRD patterns of the catalysts. *XRD* X-ray diffraction

SEM/TEM

The micro-morphologies of the catalysts and detailed internal geometrical structure of the catalysts were investigated by SEM and TEM and the results are shown in Fig. 4, The SEM images of the MnOx, Ce–MnOx and Co–MnOx catalysts exhibited similar nanoparticle and microsphere structures. However, the morphology of Fe–MnOx showed nanosheet-resemble flower-like structure. The TEM images of the Ce–MnOx and Fe–MnOx displayed hollow microsphere and flower-like nanosheet structure, respectively [19]. The TEM images of the MnOx, Co–MnOx catalysts exhibited similar nanosheet cluster structures. The crystal structure could affect the exposure of density oxygen atoms on the surface of the catalyst, thus affecting the catalytic oxidation activity of the catalyst.

XPS

XPS was applied to analyze the surface chemical states of the catalysts, and the results are shown in Fig. 5 and Table 2. The presence of Mn, Ce, Co, Fe and O in MnOx, Ce–MnOx, Co–MnOx and Fe–MnOx was confirmed in the XPS survey spectra (Fig. 5a). As depicted in Fig. 5b, the binding energies of the Mn 2p 3/2 peaks located at ca. 640.1±0.1 eV, ca. 641.5±0.3 eV and 643.0±0.3 eV are ascribed to Mn^{2+}, Mn^{3+}, and Mn^{4+}, respectively [6, 17, 19]. As shown in Table 2, the atomic ratios of Mn^{3+}/Mn and Mn^{4+}/Mn on the surfaces of the catalysts were calculated by XPS spectra using XPS PEAK. After the addition of Ce, Co, and Fe, the atomic ratios of Mn^{3+}/Mn increased from 48.89% to 66.73%, and a higher Mn^{3+}content enhanced the catalytic oxidation of VOCs [17]. However, Mn^{3+} was the dominant valence state present on the catalyst surface. Generally, metal ions with a larger percentage of high valence states were the dominant factors affecting catalytic performance at low temperatures [6].

The O 1s spectra of the catalysts are presented in Fig. 5c. There were three distinct peaks located at ca. 529.0–530.0 eV, ca. 530.1–531.5 eV, and 532.0–533.0 eV that were attributed to lattice oxygen (O_α), surface adsorbed oxygen (O_β) and water and carbonate species (O_γ), respectively [19]. The molar ratio of O_β/O_{total} was obtained by quantitative calculation of the corresponding peak areas.

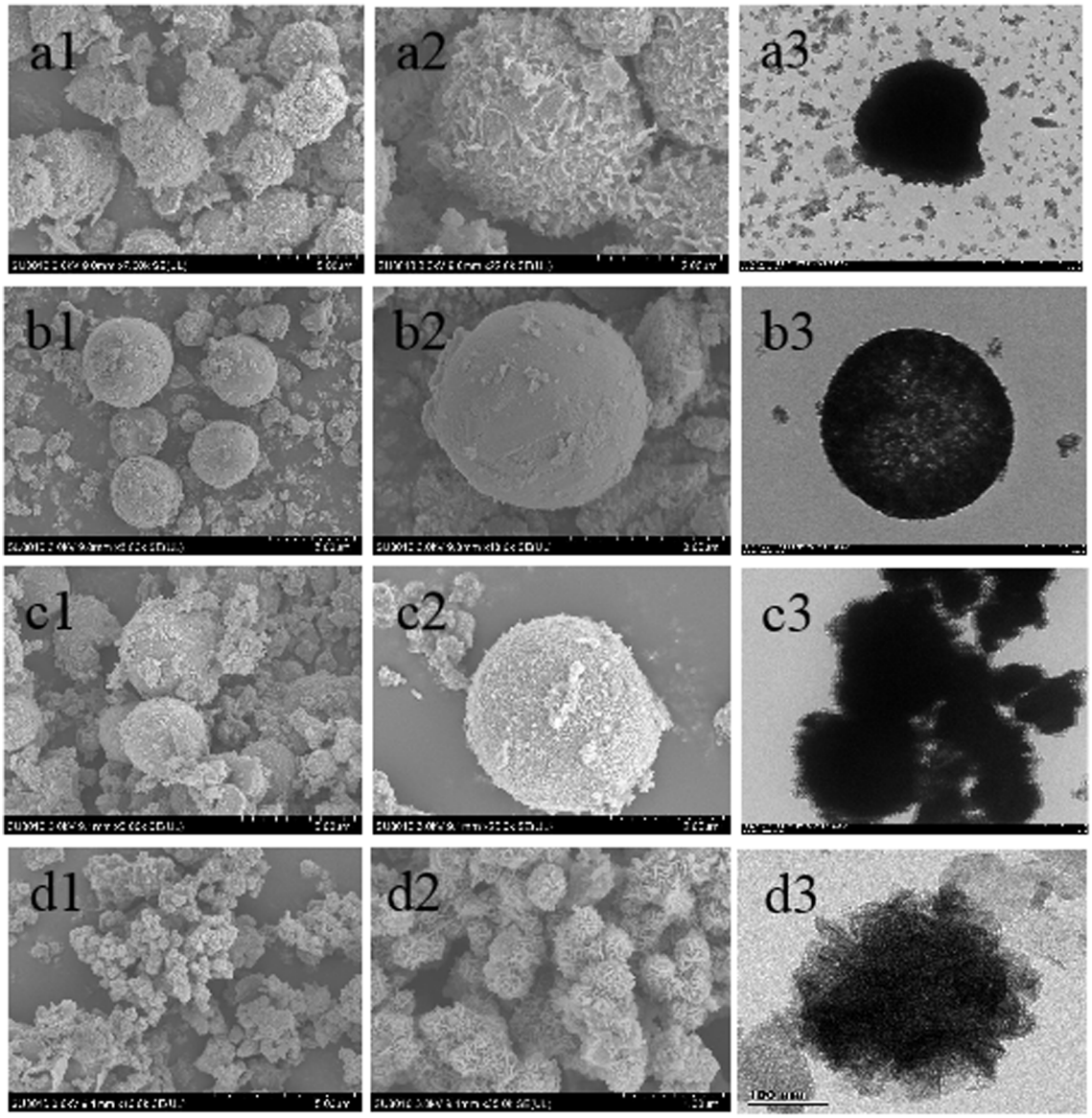

Fig. 4 SEM (Columns **1** and **2**) and TEM (Column **3**) images of MnOx (**a1**–**a3**), Ce–MnOx (**b1**–**b3**), Co–MnOx (**c1**–**c3**), Fe–MnOx (**d1**–**d3**). *SEM* scanning electron microscope, *TEM* transmission electron microscope

The O_β/O_{total} ratio of Fe–MnOx was higher than that of the other catalysts, Previous reports revealed that more surface absorbed oxygen (O_β) is beneficial to catalytic oxidation reaction [6]; hence, it was indicated that Mn^{4+} and surface-absorbed oxygen play key roles in the catalytic oxidation of 1,2-DCB [20].

NH_3-TPD

NH_3-TPD experimental results of the catalysts are shown in Fig. 6. The acidic sites are generally classified into three categories: weak acidity (<200 °C), moderate acidity (200–400 °C), and strong acidity (>400 °C) [21]. More specifically, MnOx exhibited an obvious desorption peak at 582.0 °C, while Ce–MnOx exhibited a strong NH_3 desorption peak at 489.7 °C, indicating that there were more acid sites on the Ce–MnOx catalyst. A broad and weak peak at 201.6 °C was shown on the Co–MnOx catalyst. An overlapping NH_3 desorption peak (ca.130 °C) was observed for MnOx, Ce–MnOx, and Co–MnOx. A weak peak at 115.2 °C and a strong acidity peak at 577.8 °C were observed over the Fe–MnOx catalyst. The quantitative results for acidity are summarized in Table 3. The quantities of NH_3 desorbed from weak and medium strong acid sites ranked in the order of Fe–MnOx (19.57 mmol

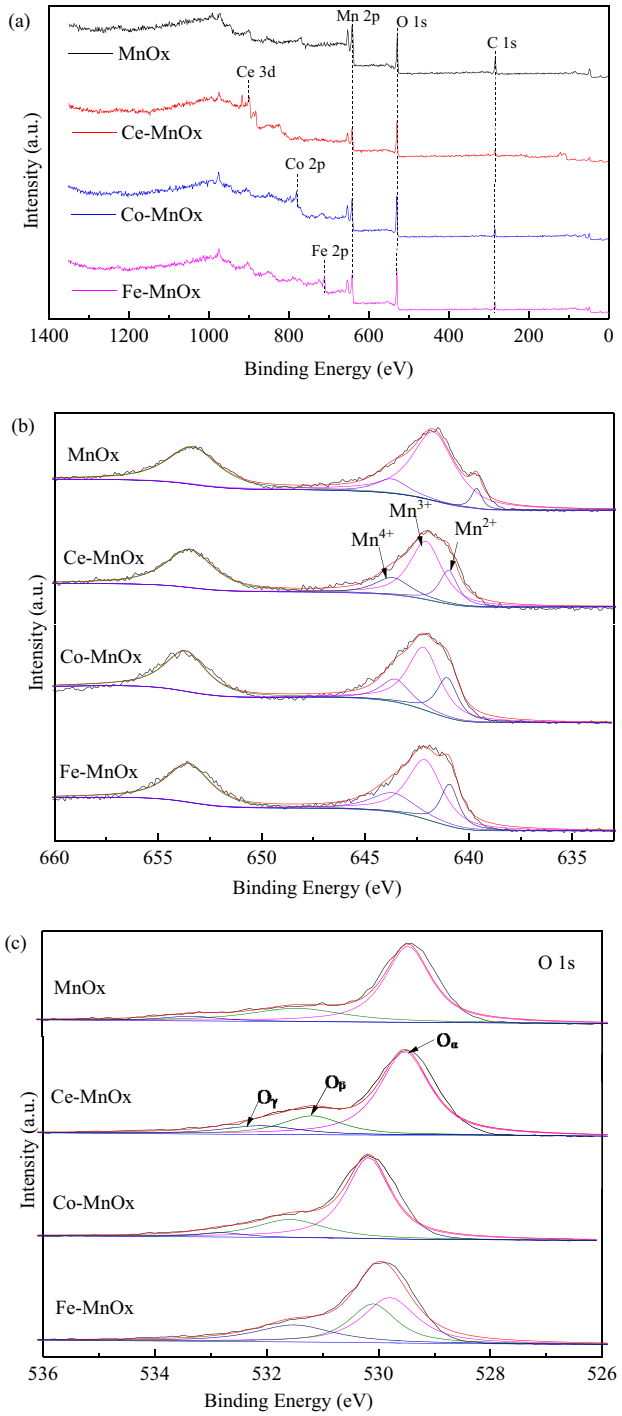

Fig. 5 XPS spectra of different samples. (**a**) XPS survey spectra, (**b**) Mn 2p, (**c**) O 1s

NH_3/g) > Co–MnOx (7.18 mmol NH_3/g) > Ce–MnOx (5.65 mmol NH_3/g) > MnO_x(5.43 mmol NH_3/g). Yang et al. reported that the acidic site amount increased significantly after the Fe species introduced in Mn–Ce/AC [22]. Previous research found that weak and medium strong acids were important for the adsorption and decomposition of 1,2-DCB; the catalytic performance of Ce–MnOx could be associated with its reducibility, oxygen vacancies, and acidity [23].

H_2-TPR

Redox properties of the catalysts are critical for DCB performance, The reducibility of the catalysts was investigated by H_2-TPR, and the results are shown in Fig. 7. The H_2-TPR profiles showed three peaks between 50 °C and 700 °C, which can be separated into the following two reduction steps: $MnO_2 \rightarrow Mn_2O_3 \rightarrow Mn_3O_4$ [24]. For the pure MnO_x catalyst, two peaks were located at approximately 367.0 °C and 473.2 °C. Ce metal doping resulted in the first H_2 reduction peak shifting to a lower temperature. The Ce–MnOx catalysts showed reduction peaks at 387.6 °C. Co and Fe metal doping resulted in the first H_2 reduction peak shifting to a higher temperature. The reduction temperature for Fe–MnOx is noticeably higher than that of other catalysts. The H_2 consumption for each catalyst is calculated in Table 4. The H_2 consumption amounts were ranked in the order Fe–MnOx > MnO_x > Co–MnOx > Ce–MnOx. The increase in H_2 consumption results in the formation of more oxygen vacancies, which facilitates oxygen mobility and enhances active catalytic reactions. After Fe doping, the low-temperature oxidation of the catalyst was enhanced and was significantly stronger than that of the single-component catalyst. Fe–MnOx exhibited the highest activity due to its low reduction temperature among these four catalysts [25].

Catalytic activity

Catalytic conversion of 1,2-DCB

The catalytic activity of as-prepared catalysts for 1,2-DCB removal is shown in Fig. 8 as a function of temperature.

Table 2 Surface element relative percentage of the catalysts

Catalysts	Mn/*M* atomic ratio (*M* = Ce, Co, Fe)	Percent of valence state %					
		Mn^{2+}	Mn^{3+}	Mn^{4+}	O_α	O_β	O_γ
MnOx	–	14.82	48.89	36.29	69.39	25.28	5.33
Ce–MnOx	0.3156	–	66.73	33.27	69.81	19.10	11.09
Co–MnOx	1.135	6.81	57.58	35.61	70.81	25.15	4.04
Fe–MnOx	1.095	8.89	60.58	30.53	43.53	32.68	23.79

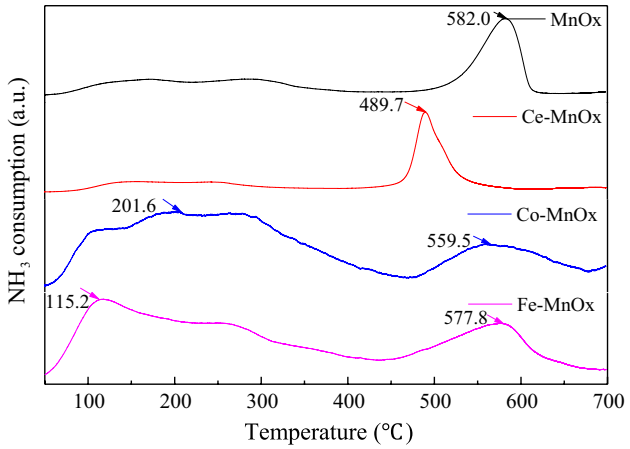

Fig. 6 NH_3-TPD profiles for the catalysts. *NH_3-TPD* ammonia temperature programmed desorption

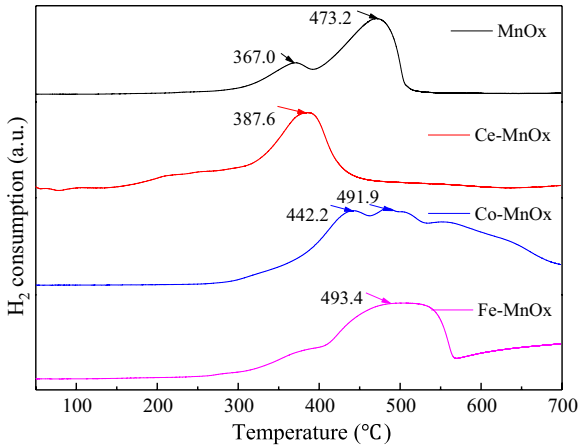

Fig. 7 H_2-TPR profiles of the catalysts. *H_2-TPR* H_2 temperature-programmed reduction

The MnOx and Co–MnOx exhibited comparable activity with T_{90} (the temperature needed for 90% conversion) of ca. 340 °C for 1,2-DCB removal. Cai et al. revealed that the Co/Mn catalyst presented the highest activity for 1,2-DCB with T_{90} of 347 °C [10]. After the addition of Ce and Fe, the conversion profile totally shifted towards lower temperatures, with T_{90} at ca. 310 °C for 1,2-DCB removal. Zhao et al. reported that Ce–MnOx rods prepared by the hydrothermal method exhibit the best destructive activity of 1,2-DCB with T_{90} at 346 °C [23]. Ma et al. reported that Fe–Mn_{20} synthesized by a hard template method achieved 69.3% of DCB conversion at 250 °C [9]. However, for the Fe–MnOx catalyst, the 1,2-DCB removal efficiency was 81.69% at 240 °C, which is higher than that of the other catalysts. The activity results are consistent with the results of O 1s in XPS and H_2-TPR.

Catalytic conversion of furan

The catalytic activity of as-prepared catalysts for furan removal is shown in Fig. 9 as a function of temperature. Furan conversion increased with increasing temperature. T_{90} is between 180 °C and 240 °C. The T_{90} ranking of catalysts is as follows: Fe–MnOx < MnOx < Ce–MnOx < Co–MnOx. Fe–MnOx exhibited the best catalytic activity. The removal efficiency of furan was 84% at 180 °C for Fe–MnOx. Compared with the 1,2-DCB oxidation process, T_{90} decreased to 180 °C for Fe–MnOx. At lower temperatures, Fe–MnOx has higher activity than other catalysts for furan removal. Thus the adsorption and oxidation behavior of furan is different from what is observed in the case of 1,2-DCB. The structures, morphologies, promotion of acidity and mobility of oxygen with the addition of Ce, Co, and Fe might be attributed to the higher activity at low temperatures [18, 21].

Simultaneous removal of 1,2-DCB and furan

Simultaneous removal of 1,2-DCB and furan tests were conducted at 120–360 °C. Figure 10 presents the catalytic activity of the catalysts for the simultaneous removal of 1,2-DCB and furan. Fe–MnOx exhibited better performance than Ce–MnOx. It was found that 1,2-DCB and furan compete for the active sites on the catalysts. Furan was adsorbed first, and the active sites were blocked such that 1,2-DCB could not be adsorbed. 1,2-DCB removal was obviously inhibited at low temperature (below 270 °C) because the active sites were first occupied by furan. The basic oxygen of furan adsorbed strongly on the acidic sites of catalyst, and the catalytic reaction was promoted [3].

Table 3 Acidic properties of the catalysts

Sample	NH_3 consumption (mmol NH_3/g)						Experimental NH_3 consumption of catalyst (mmol NH_3/g)
	Position (°C)	Peak 1	Position (°C)	Peak 2	Position (°C)	Peak 3	
MnOx	139.2	3.014	296.1	2.413	582.0	14.268	19.695
Ce–MnOx	141.1	3.101	256.4	2.551	489.7	25.849	31.501
Co–MnOx	135.7	1.370	201.6	5.811	559.5	1.655	8.836
Fe–MnOx	115.2	19.570	–	–	577.8	6.724	26.294

Table 4 Redox properties of the catalysts

Sample	H_2 consumption (mmol H_2/g)						Experimental H_2 consumption of catalyst (mmol H_2/g)
	Position (°C)	Peak 1	Position (°C)	Peak 2	Position (°C)	Peak 3	
MnOx	367.0	5.379	473.2	35.44	–	–	40.819
Ce–MnOx	249.2	1.923	387.6	16.08	–	–	18.003
Co–MnOx	442.2	6.554	491.9	8.986	558.3	5.366	20.906
Fe–MnOx	493.4	48.25	694.8	7.139	–	–	55.389

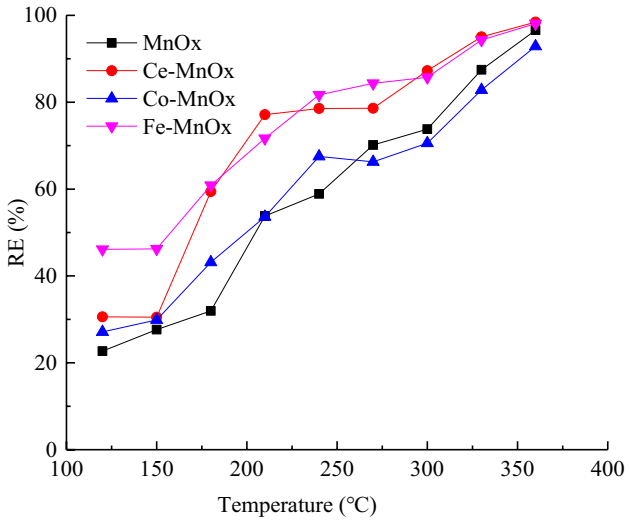

Fig. 8 Catalytic activity for 1,2-DCB removal. *1,2-DCB* 1,2-dichlorobenzene, *RE* removal efficiency

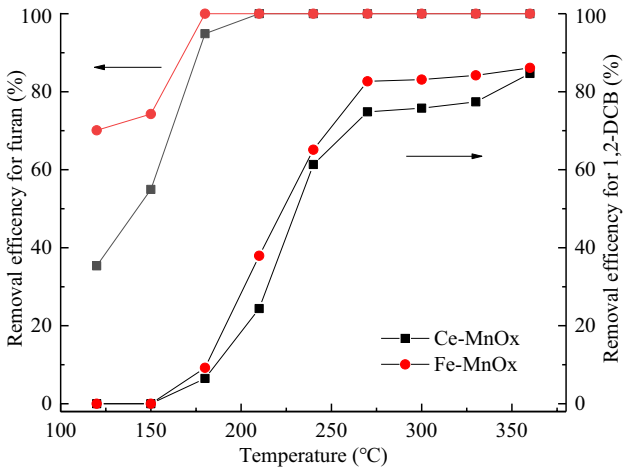

Fig. 10 Catalytic activity for simultaneous removal of 1,2-DCB and furan

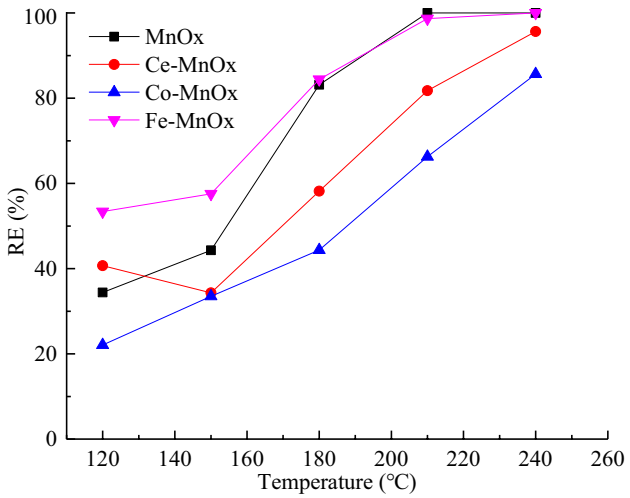

Fig. 9 Catalytic activity for furan removal

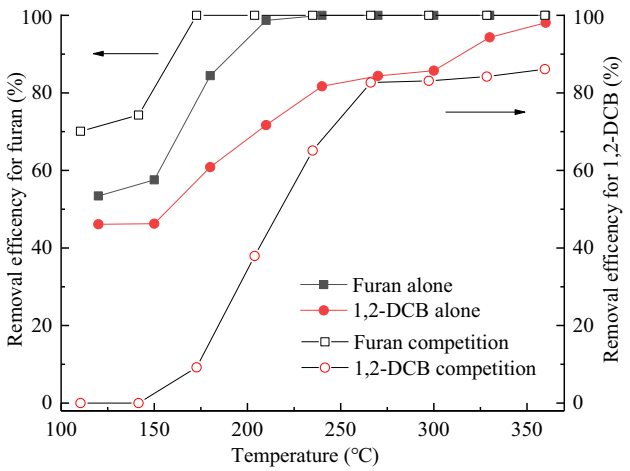

Fig. 11 Competition tests between 1,2-DCB and furan on Fe–MnOx

Figure 11 presents the catalytic performance for chlorobenzene and furan, alone and in competition. Comparing the catalytic performance for chlorobenzene and furan alone, 1,2-DCB conversion was inhibited by the presence of furan in the flow; however, furan conversion was evidently promoted. The conversion reached 46% at 150 °C when there was only 1,2-DCB in the flow. In the case of the competition test, no 1,2-DCB is removed from the flow at 150 °C, and the conversion curves shift towards higher temperatures. With the increasing temperature, the carbonaceous reaction products deposited on the surface begin to decompose, and 1,2-DCB can occupy the active site for catalytic oxidation [2].

Stability of the catalysts

The catalytic stability of catalysts is very important for commercial utilization. The stability of MnOx, Ce–MnOx, Co–MnOx, and Fe–MnOx for 1,2-DCB catalytic oxidation was evaluated at 180 °C and 300 °C. The results are shown in Fig. 12. The Fe–MnOx and Ce–MnOx catalysts exhibited higher stability at 300 °C. After 300 min, the removal efficiency was above 70%. However, the Ce–MnOx catalyst presented the highest stability at 180 °C, and the removal efficiency was above 37% after 180 min. The reason for the decline may be that strong adsorption of chlorine species would have blocked active sites [26]. As shown in Fig. 13, the stability of MnOx, Ce–MnOx, Co–MnOx and Fe–MnOx for furan catalytic oxidation was evaluated at 180 °C, and after 300 min, the removal efficiency of Fe–MnOx was approximately 60% at 180 °C. These results confirmed that Fe–MnOx catalysts are promising and efficient catalysts at low temperatures for the catalytic oxidation of Cl-VOC and furan.

Selectivity

In the 1,2-DCB oxidation reaction, the inorganic products include CO_2, CO, H_2O, HCl, and Cl_2 [27]. CO_2, CO, and HCl selectivity represents the important performance of a catalyst for catalytic oxidation of 1,2-DCB. As presented in Fig. 14a, the CO_2/CO yield of Ce–MnOx was higher than that of the others in the range 180–360 °C. The dominant products in the effluent gas of MnOx, Ce–MnOx, Co–MnOx, and Fe–MnOx catalysts showed a similar trend in the range 180–360 °C. The CO_2/CO yield increased with temperature. This result was consistent with that reported in a previous study [27]. In comparison with MnOx, the selectivity of CO_2/CO showed a slight increase after the addition of Ce, Co, and Fe. As shown in Fig. 14b, HCl in the effluent gas of catalysts shows a similar change in trend in the temperature range

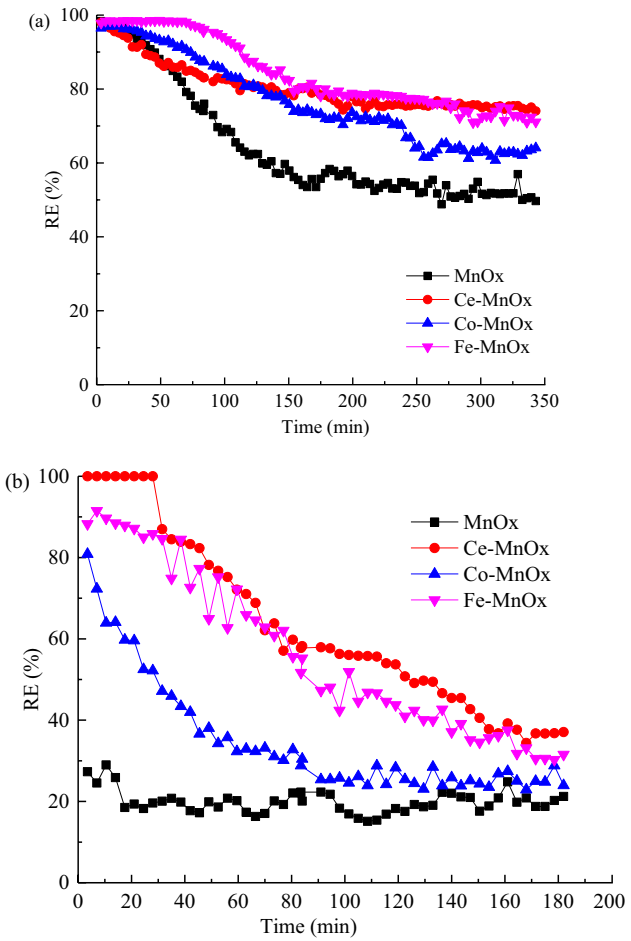

Fig. 12 Stability tests of catalysts for 1,2-DCB removal (**a**) 300 °C, (**b**) 180 °C

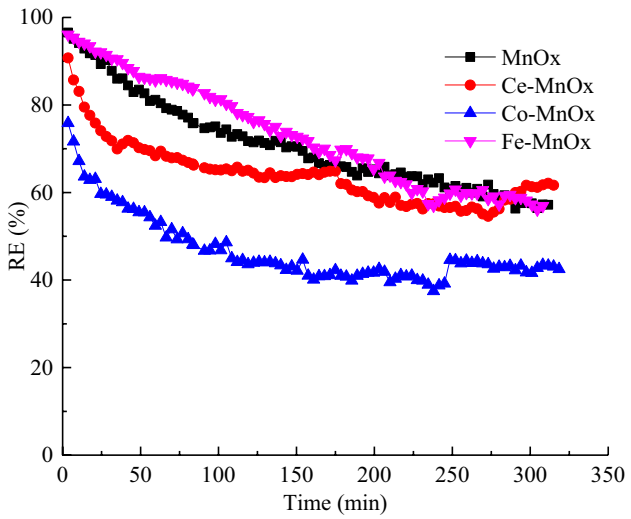

Fig. 13 Stability tests of catalysts for furan removal at 180 °C

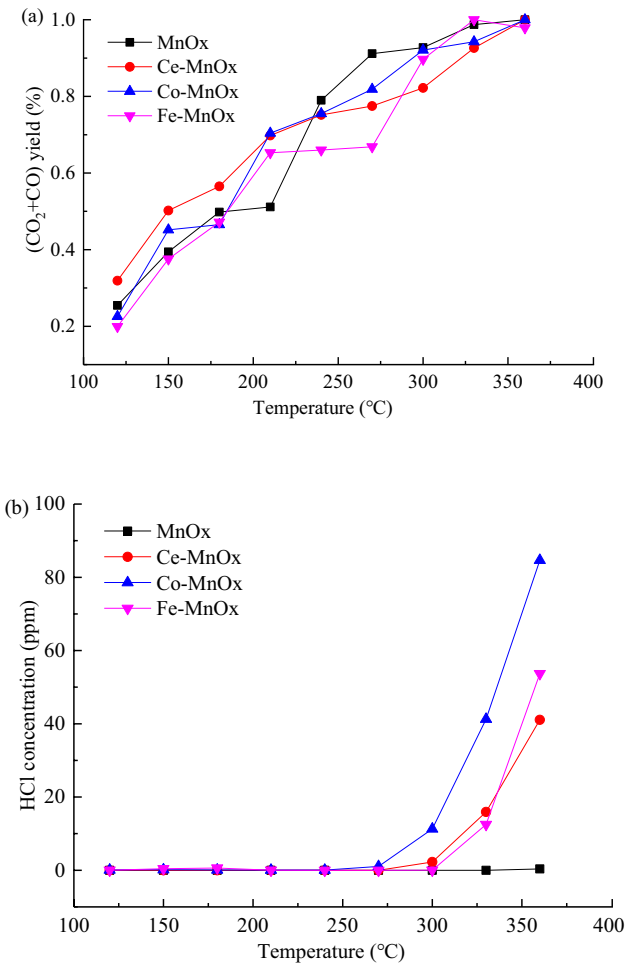

Fig. 14 The product yield over catalysts. (**a**) CO_2/CO, (**b**) HCl

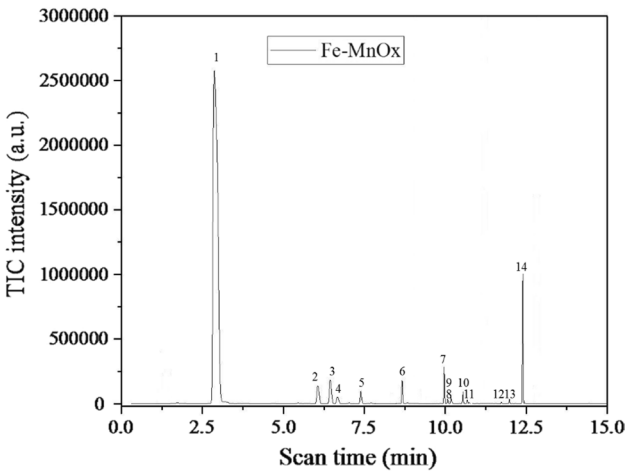

Fig. 15 GC–MS analyses of the intermediate products for the Fe–MnOx catalyst

of 120–360 °C. The concentration of HCl was below 270 °C, whereas it increased rapidly at 300 °C. The HCl concentration in the tail gas of catalytic oxidation of Co–MnOx and Fe–MnOx catalysts was higher than that of other catalysts.

Products and mechanism

Simultaneous removal of 1,2-DCB and furan was carried out on the catalyst Fe–MnOx at 300 °C. The effluent gas of the reaction after 2 h was adsorbed on an adsorption tube (Tenax) for 30 min. The byproducts in the adsorption tube were desorbed by thermal analysis and a desorption device and then analyzed by GC–MS. As shown in Fig. 15 and Table 5, furan was easily absorbed and deposited on the adsorption tube. Furan and 1,2-DCB were the major components. The main byproducts in the 1,2-DCB and furan oxidation process ranked as follows: trichloromethane > carbon tetrachloride > chlorobenzene > toluene > butynal > 3-heptanone > *p*-xylene > ethylbenzene > 2,5-dihydro-3-methyl-furan > 3-hexanol > decane.

The reaction paths were proposed based on the byproducts detected by GC/MS and the Gasmet FT-IR gas analyzer. (1) On the Lewis sites of the Fe–MnOx catalyst, furan is adsorbed prior to 1,2-DCB, and then it is partially oxidized to butynal, 2,5-dihydro-3-methyl-furan. (2) 1,2-DCB was absorbed on the Fe–MnOx catalyst; then, the C–Cl bond was abstracted by nucleophilic substitution of the oxygen from OH groups and the formation of the chlorophenoxy species. (3) 1,2-DCB reacts with active oxygen species to generate oxygenated hydrocarbons, and then decomposes to aldehydes or ketones. (4) A fragment of 1,2-DCB was oxidized to chlorinated hydrocarbons via electrophilic substitution. (5) These byproducts could undergo further oxidization to the final products, namely CO_2, H_2O, HCl and so on [26–28].

Conclusions

In summary, Mn-based bimetallic oxides were synthesized by the solvothermal method. The structure and physicochemical properties of catalysts formed by different transition metals showed great differences. The catalytic activity and stability of catalysts on 1,2-DCB and furan oxidation were tested. Fe–MnOx catalysts exhibited better catalytic activity. The main reason for the superior catalytic activities of Fe–MnOx were attributed to their unique structure, Mn-enriched surface and amount of active oxygen. Compared with the catalytic performance for chlorobenzene and furan alone, 1,2-DCB conversion was inhibited by the presence of furan in the flue gas; however, furan conversion was promoted. Stability tests were used to evaluate the deactivation rate in all catalysts.

Table 5 Intermediate products of 1,2-DCB and furan on the Fe–MnOx catalyst

Label	Molecular formula	Name of compound	Molecular structure	Percentage (%)
1	C_4H_4O	Furan		83.6
2	$CHCl_3$	Trichloromethane	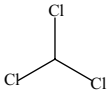	2.2
3	CCl_4	Cabon Tetrachloride	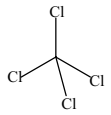	2.8
4	C_4H_8O	Butynal	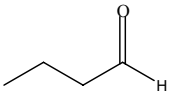	0.82
6	$CHCl_3$	Trichloromethane	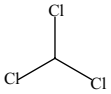	1.0
7	C_7H_8	Toluene	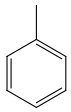	1.24
8	C_6H_5Cl	Chlorobenzene	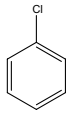	1.57
9	C_8H_{10}	Ethylbenzene	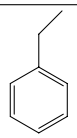	0.21
10	C_8H_{10}	P-xylene	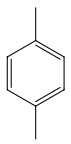	0.44
11	$C_7H_{14}O$	3-Heptanone	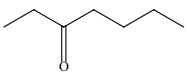	0.55
12	$C_6H_{14}O$	3-Hexanol	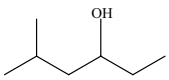	0.16
13	$C_{10}H_{22}$	Decane	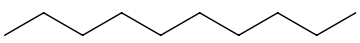	0.15
14	C_5H_8O	2,5-dihydro-3- methyl-furan		0.19
17	$C_6H_4Cl_2$	1,2- dichlorobenzene	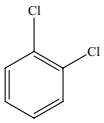	5.06

The selectivity of Fe–MnOx towards CO_2 and CO reached 90% at 300 °C. Intermediate products of the 1,2-DCB and furan oxidation process over Fe–MnOx were analyzed by GC–MS, and then the reaction paths were proposed.

Acknowledgements This work was supported by the Natural Science Foundation of Zhejiang Province (No. LY21E060007), and the National Natural Science Foundation of China (No. 51976192, No. 52006191). Additionally, a special thanks to Chengetai Portia Makwarimba who helped to improve the clarity of this manuscript.

Declarations

Conflict of interest Jianhua Yan is the Editor-in-Chief of Waste Disposal & Sustainable Energy. The authors declare that they have no conflict of interest.

References

1. Ssebugere, P., Sillanpää, M., and Matovu, H. 2019. Human and environmental exposure to PCDD/Fs and dioxin-like PCBs in Africa: a review. *Chemosphere* 223: 483–493.
2. Debecker, D.P., Bertinchamps, F., Blangenois, N., et al. 2007. On the impact of the choice of model VOC in the evaluation of V-based catalysts for the total oxidation of dioxins: furan vs. Chlorobenzene. *Applied Catalysis B: Environmental* 74: 223–232.
3. Debecker, D.P., Delaigle, R., Eloy, P., et al. 2008. Abatement of model molecules for dioxin total oxidation on V_2O_5–WO_3/TiO_2 catalysts: the case of substituted oxygen-containing VOC. *Journal of Molecular Catalysis A: Chemical* 289: 38–43.
4. Zhao, H., Li, H.C., Pan, Z.F., et al. 2020. Design of CeMnCu ternary mixed oxides as soot combustion catalysts based on optimized Ce/Mn and Mn/Cu ratios in binary mixed oxides. *Applied Catalysis B: Environmental* 268: 118422.
5. Du, C.C., Lu, S.Y., Wang, Q.L., et al. 2018. A review on catalytic oxidation of chloroaromatics from flue gas. *Chemical Engineering Journal* 334: 519–544.
6. Shi, Y.R., Yi, H.H., Gao, F.Y., et al. 2021. Evolution mechanism of transition metal in NH_3-SCR reaction over Mn-based bimetallic oxide catalysts: Structure-activity relationships. *Journal of Hazardous Materials* 413: 125361.
7. Tang, A.D., Hu, L.Q., Yang, X.H., et al. 2016. Promoting effect of the addition of Ce and Fe on manganese oxide catalyst for 1,2-dichlorobenzene catalytic combustion. *Catalysis Communications* 82: 41–45.
8. Du, J.P., Qu, Z.P., Dong, C., et al. 2018. Low-temperature abatement of toluene over Mn–Ce oxides catalysts synthesized by a modified hydrothermal approach. *Applied Surface Science* 433: 1025–1035.
9. Ma, X.D., Wen, J.X., Guo, H.W., et al. 2020. Facile template fabrication of Fe–Mn mixed oxides with hollow microsphere structure for efficient and stable catalytic oxidation of 1,2-dichlorobenzene. *Chemical Engineering Journal* 382: 122940.
10. Cai, T., Huang, H., Deng, W., et al. 2015. Catalytic combustion of 1,2-dichlorobenzene at low temperature over Mn-modified Co_3O_4 catalysts. *Applied Catalysis B: Environmental* 166–167: 393–405.
11. Wang, Y., Deng, W., Wang, Y.F., et al. 2018. A comparative study of the catalytic oxidation of chlorobenzene and toluene over Ce–Mn oxides. *Molecular Catalysis* 459: 61–70.
12. Zhang, X.J., Zhao, J.G., Song, Z.X., et al. 2020. The catalytic oxidation performance of toluene over the Ce–Mn–Ox catalysts: effect of synthetic routes. *Journal of Colloid and Interface Science* 562: 170–181.
13. Khaleel, A., and Al-Nayli, A. 2008. Supported and mixed oxide catalysts based on iron and titanium for the oxidative decomposition of chlorobenzene. *Applied Catalysis B: Environmental* 80: 176–184.
14. Qi, G.S., and Yang, R.T. 2003. Low-temperature selective catalytic reduction of NO with NH_3 over iron and manganese oxides supported on titania. *Applied Catalysis B: Environmental* 44: 217–225.
15. Cheng, Z., Chen, Z., Li, J.R., et al. 2018. Mesoporous silica-pillared clays supported nanosized Co_3O_4–CeO_2 for catalytic combustion of toluene. *Applied Surface Science* 459: 32–39.
16. Hu, Z.P., Zhu, Y.P., Gao, Z.M., et al. 2016. CuO catalysts supported on activated red mud for efficient catalytic carbon monoxide oxidation. *Chemical Engineering Journal* 302: 23–32.
17. Liu, J.X., Cheng, H.F., Tan, J.B., et al. 2020. Solvent-free rapid synthesis of porous CeWOx by a mechanochemical self-assembly strategy for the abatement of NOx. *Journal of Materials Chemistry A* 8: 6717–6731.
18. Chen, J., Chen, X., Xu, W.J., et al. 2018. Homogeneous introduction of CeOy into MnOx-based catalyst for oxidation of aromatic VOCs. *Applied Catalysis B: Environmental* 224: 825–835.
19. Meng, D.M., Zhan, W.C., Guo, Y., et al. 2016. A highly effective catalyst of Sm–Mn mixed oxide for the selective catalytic reduction of NOx with ammonia: effect of the calcination temperature. *Journal of Molecular Catalysis A: Chemical* 420: 272–281.
20. Chen, J.H., Shen, M.Q., Wang, X.Q., et al. 2013. The influence of nonstoichiometry on $LaMnO_3$ perovskite for catalytic NO oxidation. *Applied Catalysis B: Environmental* 134–135: 251–257.
21. Deng, W., Tang, Q.X., et al. 2020. Low temperature catalytic combustion of chlorobenzene over cobalt based mixed oxides derived from layered double hydroxides. *Applied Catalysis B: Environmental* 278: 119336.
22. Yang, J., Ren, S., Zhang, T.S., et al. 2020. Iron doped effects on active sites formation over activated carbon supported Mn–Ce oxide catalysts for low-temperature SCR of NO. *Chemical Engineering Journal* 379: 122398.
23. Zhao, H.J., Dong, F., Han, W.L., et al. 2019. Study of morphology-dependent and crystal-plane effects of CeMnOx catalysts for 1,2-dichlorobenzene catalytic elimination. *Industrial and Engineering Chemistry Research* 58: 18055–18064.
24. Lin, X.T., Li, S.J., He, H., et al. 2018. Evolution of oxygen vacancies in MnOx–CeO_2 mixed oxides for soot oxidation. *Applied Catalysis B: Environmental* 223: 91–102.
25. Liang, Y.N., Mao, D.S., Guo, X.M., et al. 2021. Solvothermal preparation of CuO–ZnO–ZrO_2 catalysts for methanol synthesis via CO_2 hydrogenation. *Journal of the Taiwan Institute of Chemical Engineers* 121: 81–91.
26. Long, G.Y., Chen, M.X., Li, Y.J., et al. 2019. One-pot synthesis of monolithic Mn–Ce–Zr ternary mixed oxides catalyst for the catalytic combustion of chlorobenzene. *Chemical Engineering Journal* 360: 964–973.
27. Li, N., Cheng, J., Xing, X., et al. 2020. Distribution and formation mechanisms of polychlorinated organic by-products upon the catalytic oxidation of 1,2-dichlorobenzene with palladium-loaded catalysts. *Journal of Hazardous Materials* 393: 122412.
28. Qiu, J., Peng, Y.Q., Tang, M.H., et al. 2021. Catalytic activity, selectivity, and stability of co-precipitation synthesized Mn–Ce mixed oxides for the oxidation of 1,2-dichlorobenzene. *Environmental Science and Pollution Research* 28: 65416–65427.